Biophysical Journal, Volume *115*

Supplemental Information

Theoretical Study on Gold-Nanorod-Enhanced Near-Infrared Neural Stimulation

Kyungsik Eom, Kyung Min Byun, Sang Beom Jun, Sung June Kim, and Jonghwan Lee

Laser induced heat

When shining light with the 980-nm wavelength on a GNR located near the neural cell membrane, the light energy is absorbed by the GNR. Since neural tissue is transparent in the near-infrared region compared to GNRs, we assumed light interacts only with GNRs to generates thermal heat. The amount of heat generated from the single GNR can be solved by using Eq. 1, (1)

$$Q_{GNR} = \frac{C_{abs} I_{laser}}{V} \tag{1}$$

where, C_{abs} is the absorption cross-section area of the single GNR, I_{laser} is the laser intensity [W·m^{-2}], and V is the volume of GNR. The absorption cross-section area (C_{abs}) was approximately determined using the Gans theory (2, 3) as Eq. 2-4 while assuming the geometry of GNR as a spheroid with the diameter and the length of 15.3 nm and 80.4 nm, respectively.

$$C_{ext} = \frac{2\pi V {\varepsilon_m}^{3/2}}{3\lambda} \sum_j^3 \frac{\left(\frac{1}{P_j}\right)^2 \varepsilon_2}{\left(\varepsilon_1 + \frac{1-P_j}{P_j}\varepsilon_m\right)^2 + {\varepsilon_2}^2} \tag{2}$$

$$C_{sca} = \frac{8\pi^3 V {\varepsilon_m}^2}{3\lambda^4} \sum_j^3 \frac{\left(\frac{1}{P_j}\right)^2 [(\varepsilon_1 - \varepsilon_m)^2 + {\varepsilon_2}^2]}{\left(\varepsilon_1 + \frac{1-P_j}{P_j}\varepsilon_m\right)^2 + {\varepsilon_2}^2} \tag{3}$$

$$C_{ext} = C_{abs} + C_{sca} \tag{4}$$

where, ε_m is the dielectric constant of the surrounding medium, λ is the wavelength of the light, ε_1 and ε_2 are the real and the imaginary part of the gold dielectric function, respectively, P_j is depolarization factor for three axes, C_{ext} is the extinction cross section area, C_{sca} scattering cross section area, and P_j is the depolarization factor for three axes *A*, *B* and *C* (*A*>*B*=*C*).

$$P_z = \frac{1-e^2}{e^2}\left[\frac{1}{2e}\ln\left(\frac{1+e}{1-e}\right) - 1\right], \qquad e = \sqrt{1 - \left(\frac{B}{A}\right)^2}$$

$$P_B = P_C = \frac{1 - P_A}{2}$$

The heat generated from the GNR diffuses and thus increase the temperature in the plasma membrane. Prior to simulating the temperature profile at the plasma membrane, we assumed followings: (1) GNRs are uniformly distributed as a single layer of GNRs with an empirical parameter of the "coverage" *c* and the distance from the membrane of 100 nm (4). (2) Macroscopically, heat generated from GNRs is uniformly distributed along the GNR layer. (3) Heat generated from GNRs is considered as a constant heat source, Q_{GNR}. (4) The heat flows out of the GNR sheet along the *x*-axis, perpendicular to the sheet. Based on these assumptions, the temperature profile can be calculated by using the 1-dimensional heat diffusion equation (Eq. 5) (5),

$$\frac{1}{\alpha}\frac{\partial T}{\partial t} = \frac{\partial^2 T}{\partial x^2} + \frac{cQ_{GNR}}{k} \qquad (5)$$

where, α is the thermal diffusivity of cerebrospinal fluid (CSF, 1.48×10^{-7} [$m^2 \cdot s^{-1}$]), k is the thermal conductivity of CSF (0.57 [$W \cdot m^{-1} \cdot K^{-1}$]), the external heat source of Q_{GNR}, x is the distance between center of the GNRs sheet [m], t is the time [s], T is the temperature [K], and c is the GNRs coverage. Here, the "coverage" c is deduced from the laser parameters and its corresponding thermal profile results reported in previous publication by Eom et al. (6), to be 0.031.

Absorption cross-sectional area of randomly oriented GNRs

We determined how the orientation of GNRs impacts on the C_{abs}. Unlike the spherical gold nanoparticles, the GNR has a directional selectivity upon the incoming light to generate localized surface plasmon resonance (LSPR). Especially when the direction of electric-field (E-field) of incoming light is matched to the long-axis of GNR, the maximum absorption cross-sectional area ($\overline{C_{abs}}$) is created and thereby inducing an efficient photothermal conversion. However, C_{abs} decreases from the $\overline{C_{abs}}$ if the GNR is tilted with respect to the direction of E-field (Fig. S1). $\overline{C_{abs}}$ will be scaled by $\cos^2\theta$ when the GNR is rotated by θ, whereas C_{abs} has negligible effect on the GNR rotation in the φ direction since E-field influences the same manner regardless of the φ direction especially where the wavelength of light is much bigger than the GNR. If the probability of a GNR having specific direction of θ and φ is $p(\theta,\varphi)$ then C_{abs} can be calculated as Eq. 6.

$$C_{abs} = \int_0^{\pi}\int_0^{2\pi} \overline{C_{abs}}\, cos^2(\theta) p(\theta,\varphi) r^2 \sin\theta \, d\varphi d\theta \tag{6}$$

where r is the unit length. For our case we could considered GNRs are randomly oriented and thereby the $p(\theta,\varphi)$ can be deduced as '$\frac{1}{4\pi r^2}$' by the relation of $1 = \int_0^{\pi}\int_0^{2\pi} p(\theta,\varphi) r^2 \sin\theta \, d\varphi d\theta$. As a result, C_{abs} is '$\frac{\overline{C_{abs}}}{3}$'.

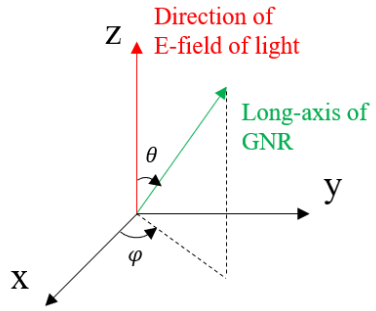

FIGURE S1. Orientations of electric-field of incident light and the long-axis of GNR.

As in Eq. 7, the average heat generated by the GNRs is proportional to the coverage 'c', depending on how many GNRs locate per unit area of the membrane, and the 'absorption cross-sectional area (C_{abs})', depending on the orientation of GNRs. Since both factor have the same effect (scaling) on C_{abs}, we chose GNR coverage to find the effect of coverage and the distance on AP generation.

$$cQ_{GNR} = c\frac{C_{abs}I_{laser}}{v_p} \tag{7}$$

Modeling of TRPV1 channel

The current through the TRPV1 channel is estimated using the function that combines linear conductance and Boltzmann activation term ($I_{TRPV1} = G_{TRPV1}(V - E_{TRPV1}) / \left[1 + \exp\left(\frac{-(V_{1/2} - V)}{RT/zF}\right)\right]$). The E_{TRPV1} of non-selective cation TRPV1 channel was calculated using the Goldman equation. From the previous publication reported by Voet el al., the value of G_{TRPV1} and the equation of $V_{1/2}$ were deduced and the z were obtained (7).

The reversal potential of TRPV1 (E_{TRPV1}) channel is calculated as –10.5 mV and the derivation is shown in the below 'Reversal potential of TRPV1 channel' section. The conductance of TRPV1 channel is calculated using the equation $G_{TRPV1} = I/[(V - E_{TRPV1}) \times \pi r^2]$. From the previous report by Voets et al. (7), the maximum current experimentally obtained upon –60 mV voltage ramp at 35ºC are employed. If we assume the shape of a cell as a sphere with 15 µm radius, then the G_{TRPV1} is computed as 1.3 $S \cdot m^{-2}$. The potential for half maximum activation ($V_{1/2}$, [V]) is determined as $V_{1/2} = 9 \times 10^{-3}(T - 309.1)$ where T is temperature [K] (7). Finally, the effective gating charge (z) is obtained as 0.71 (7).

Reversal potential of TRPV1 channel

A reversal potential of TRPV1 channel allowing multiple of cations (e.g. Ca^{2+}, Na^{+}, and K^{+}) is not simply governed by the Nernst equation. According to the Nernst-Plank equation, ion fluxes across the membrane can be decomposed into two factors: diffusional force resulting from the difference in the ionic concentration and membrane electric field on ions. The electric field is further assumed to be constant along the 'z' direction which is perpendicular to the membrane and its value equal is to the ratio of transmembrane potential (E_m) and the thickness of the membrane (L). The flux of a single ion (j_A, [mol·sec^{-1}·m^{-2}]) is represented as

$$j_A = -D_A\left(\frac{d[A]}{dz} - \frac{z_A F}{RT}\frac{E_m}{L}[A]\right) \qquad (8)$$

where, D_A is the diffusion constant of ion A [m^2·sec^{-1}], z_A is the valance of ion A, F is the faraday constant, R is the gas constant, T is the is the absolute temperature. Separating the values leads

$$\frac{d[A]}{\left(\frac{-j_A}{D_A} + \frac{z_A F}{RT}\frac{E_m}{L}[A]\right)} = dz$$

Integrate across the membrane ($z = 0$, $z = L$) yields

$$L = \frac{RTL}{FE_m z_A}\ln\left(\frac{-\frac{j_A}{D_A} + \frac{z_A F E_m}{RTL}[A]_{out}}{-\frac{j_A}{D_A} + \frac{z_A F E_m}{RTL}[A]_{in}}\right)$$

Solving for j_A results

$$j_A = \frac{z_A F E_m}{RT}\frac{D_A}{L}\left(\frac{[A]_{out} - [A]_{in}e^{\frac{z_A F E_m}{RT}}}{1 - e^{\frac{z_A F E_m}{RT}}}\right) = z_A \mu P_A\left(\frac{[A]_{out} - [A]_{in}e^{z_A \mu}}{1 - e^{z_A \mu}}\right)$$

where, μ equals to $\frac{FE_m}{RT}$ and ion permeability (P_A) is $\frac{D_A}{L}$. The electric current density [A·m^{-2}] is expressed as

$$I_A = Fq_A j_A$$

where, q_A is the sign of the ion *A*. Since the sum of electric current density for all ions (Ca^{2+}, Na^{+}, and K^{+}) is zero.

$$\begin{aligned} 0 = {} & Fq_{Na^+} z_{Na^+} \mu P_{Na^+} \left(\frac{[Na^+]_{out} - [Na^+]_{in} e^{z_{Na^+}\mu}}{1 - e^{z_{Na^+}\mu}} \right) \\ & + Fq_{K^+} z_{K^+} \mu P_{K^+} \left(\frac{[K^+]_{out} - [K^+]_{in} e^{z_{K^+}\mu}}{1 - e^{z_{K^+}\mu}} \right) \\ & + Fq_{Ca^{2+}} z_{Ca^{2+}} \mu P_{Ca^{2+}} \left(\frac{[Ca^{2+}]_{out} - [Ca^{2+}]_{in} e^{z_{Ca^{2+}}\mu}}{1 - e^{z_{Ca^{2+}}\mu}} \right) \end{aligned}$$

Applying the values of valance for each ion leads to

$$\begin{aligned} 0 = e^{2\mu} & (-2P_{Ca^{2+}}[Ca^{2+}]_{in} - P_{Na^+}[Na^+]_{in} + P_{K^+}[K^+]_{in}) \\ & + e^{\mu}(P_{Na^+}[Na^+]_{out} + P_{K^+}[K^+]_{out} - P_{Na^+}[Na^+]_{in} - P_{K^+}[K^+]_{in}) \\ & + (2P_{Ca^{2+}}[Ca^{2+}]_{out} + P_{Na^+}[Na^+]_{out} + P_{K^+}[K^+]_{out}) \end{aligned}$$

Applying the quadratic equation, potential across the membrane is computed using

$$E_m = \frac{RT}{F} ln \frac{-\beta \pm \sqrt{\beta^2 - 4\alpha\gamma}}{2\alpha}$$

where, $\alpha = -2P_{Ca^{2+}}[Ca^{2+}]_{in} - P_{Na^+}[Na^+]_{in} + P_{K^+}[K^+]_{in}$, $\beta = P_{Na^+}[Na^+]_{out} + P_{K^+}[K^+]_{out} - P_{Na^+}[Na^+]_{in} - P_{K^+}[K^+]_{in}$, and $\gamma = 2P_{Ca^{2+}}[Ca^{2+}]_{out} + P_{Na^+}[Na^+]_{out} + P_{K^+}[K^+]_{out}$.

From the previous report (8), Ca^{2+} shows the largest channel permeability while Na^{+} and K^{+} show almost same but small permeability ($P_{Ca^{2+}}/P_{Na^+} = 9.6$). Applying the permeability relation of each ion and the values in the Table S4, the potential across the membrane or the equilibrium potential for TRPV1 channel is determined as 0.01005 V ($E_m = E_{TRPV1}$).

Derivation of modified Gouy-Chapman-Stern theory

TABLE S1 Definition of variables and their corresponding values to calculate the capacitive current (9, 10).

Variable	Definition	Value	Units
V_m	Membrane potential/ potential difference between outer- and inner bulk medium	variable	[V]
$\Phi(-\delta_{bi} - \delta_i{}^s)$	Potential at the interface between the inner Stern layer and the inner diffuse layer	variable	[V]
$\Phi(-\delta_{bi})$	Surface potential at the inner lipid bilayer	variable	[V]
$\Phi(0)$	Surface potential at the outer lipid bilayer	variable	[V]
$\Phi(\delta_o{}^s)$	Potential at the interface between the outer Stern layer and the outer diffuse layer	variable	[V]
σ_i	Intrinsic charge density of inner side of lipid bilayer	−0.006	[C·m^{-2}]
σ_o	Intrinsic charge density of outer side of lipid bilayer	−0.006	[C·m^{-2}]
σ_i^s	Intrinsic charge density at the interface between the inner Stern layer and the inner diffuse layer	variable	[V]
σ_o^s	Intrinsic charge density at the interface between the outer Stern layer and the outer diffuse layer	variable	[V]
ε_{bi}	Permittivity of lipid bilayer	$2.5 \times \varepsilon_{\text{freespace}}$	[A^2·s^4·kg^{-1}·m^{-3}]
δ_{bi}	Thickness of lipid bilayer	3×10^{-9}	[m]
ε	Permittivity of electrolyte medium	$87.740 - 0.40008 \times t + 9.398(10^{-4}) \times t^2 - 1.410(10^{-6}) \times t^3$	[A^2·s^4·kg^{-1}·m^{-3}]
$c_i{}^j(-\infty)$	Concentration of *j-th* ionic species in inner bulk medium	refer Table S3	[M]
$c_o{}^j(\infty)$	Concentration of *j-th* ionic species in outer bulk medium	refer Table S3	[M]
$z_i{}^j$	Valence of *j-th* ionic species in inner electrolyte	refer Table S3	-
$z_o{}^j$	Valence of *j-th* ionic species in outer electrolyte	refer Table S3	-
$\varepsilon_i{}^s$	Permittivity of inner Stern layer	$\varepsilon/10$	[A^2·s^4·kg^{-1}·m^{-}

			^{3}]
$\boldsymbol{\varepsilon_o^s}$	Permittivity of outer Stern layer	ε/10	[$A^2 \cdot s^4 \cdot kg^{-1} \cdot m^{-3}$]
$\boldsymbol{r_i^j}$	Hydrated ionic radius of *j-th* ionic species in inner electrolyte	refer Table S3	[m]
$\boldsymbol{r_o^j}$	Hydrated ionic radius of *j-th* ionic species in outer electrolyte	refer Table S3	[m]
$\boldsymbol{\delta_i^{lipid}}$	Hydrated size of inner polar lipid head groups	0.45×10^{-9}	[m]
$\boldsymbol{\delta_o^{lipid}}$	Hydrated size of outer polar lipid head groups	0.45×10^{-9}	[m]
$\boldsymbol{\delta_i^s}$	Thickness of inner Stern layer	variable	[m]
$\boldsymbol{\delta_o^s}$	Thickness of outer Stern layer	variable	[m]

Temperature-dependent capacitance

Unlike the fixed capacitance of lipid bilayer observed at the classical Hodgkin–Huxley model (11), capacitance change is accompanied by the temperature variation due to the structure change (axial narrowing and lateral expansion) of the lipid bilayer (12). However, it is reasonable to speculate that the lipid bilayer would not be axially smaller nor laterally larger than the certain limits conferring the maximum limit of capacitance of lipid bilayer. Therefore, it is natural to assume the temperature dependence of the capacitance as $C(T) = C_{max}(1 - \beta e^{-\alpha T})$, where C_{max} is the maximum capacitance [F·m^{-2}], T is the temperature [K], α is the temperature elevation constant [K], and the β is the scaling coefficient. Since the capacitance at 6.3°C is known as $C_{initial}(= 1)$ [F·m^{-2}] (11), we obtain Eq. 9.

$$C_{bi}(T) = \frac{C_{initial}}{1-\beta}\left(1 - \beta e^{-\frac{(T-279.3)}{\alpha}}\right) \qquad (9)$$

We, then, deduced the α and β from the current response in voltage-clamped lipid bilayer (I – V relation) when stimulating using laser which was experimentally obtained by Shapiro et al (9). The stimulus intensity they used was 7.3 mJ with a pulse duration of 10 ms and it generates the roughly linear increase in temperature up to 22.2°C, followed by temperature decaying exponentially after laser illumination with a time constant of 100 ms. When the temperature elevation constant (α) and scaling coefficient (β) are 2150.5 K and 0.75, respectively, numerically calculated *I–V* response closely matched to that of the experimentally measured indicating that modeled capacitance of lipid bilayer is in good agreement with the actual capacitance (Fig. S2).

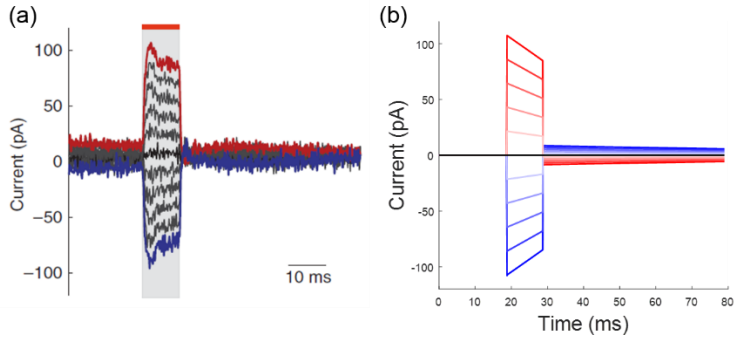

FIGURE S2. Graphs depicting (a) experimentally obtained and (b) numerically calculated *I–V* current response in voltage-clamped lipid bilayer. The holding potentials were varied from –200 mV (blue) to 200 mV (red).

Sodium, potassium, and leak current

Hodgkin-Huxley (HH) model describes the ion channels as variable conductances with respect to time and voltage. The potassium conductance is described using its maximum conductance and open probability (*n*). By contrast, sodium conductance is described by its maximum conductance, open probability of activation gate (*m*) and inactivation gate (*h*). The open probabilities of each *n*, *m*, *h* are calculated by using rate change of each close and open state (Eqs. 10) (11). All the rate constants ($\alpha_{m/n/h}$, $\beta_{m/n/h}$) were empirically derived at 279.3 K as Eqs. 11 having Q_{10} of 3. Finally, current for sodium channel, potassium channel, and leakage pathway are derived using the rate constants, the maximal conductance of each current path ($\overline{G_{K+}}, \overline{G_{Na+}}, and\ \overline{G_{Leak}}$), reversal potentials, and the membrane potential (V_m) (Eq. 13) (11). All the parameters are detailed in the Table S2.

$$\frac{dn}{dt} = \alpha_n(1-n) - \beta_n n \qquad (10)$$

$$\frac{dm}{dt} = \alpha_m(1-m) - \beta_m m$$

$$\frac{dh}{dt} = \alpha_h(1-h) - \beta_h h$$

whose, $\alpha_{n/m/h}$ and $\beta_{n/m/h}$,

$$\alpha_n = \frac{-100(100V_m + 6)}{exp(-100V_m - 6) - 1} \times 3^{\frac{T-279.3}{10}} \qquad (11)$$

$$\beta_n = 125exp(-12.5(V_m + 0.07)) \times 3^{\frac{T-279.3}{10}}$$

$$\alpha_m = \frac{-100(1000V_m + 45)}{exp(-100V_m - 4.5) - 1} \times 3^{\frac{T-279.3}{10}}$$

$$\beta_m = 4000exp\left(\frac{-1000(V_m + 0.07)}{18}\right) \times 3^{\frac{T-279.3}{10}}$$

$$\alpha_h = 70exp(50V_m + 3.5) \times 3^{\frac{T-279.3}{10}}$$

$$\beta_h = \frac{1000}{exp(-100V_m - 4) + 1} \times 3^{\frac{T-279.3}{10}}$$

The reversal potentials for sodium and potassium channel (E_{Na^+}, E_{K^+}) can be simply computed using the Nernst equation (Eq. 12).

$$E_{ion\ channel} = \frac{RT}{zF} ln\left(\frac{C_{out}}{C_{in}}\right) \quad (12)$$

where, R is gas constant, T is absolute temperature, z is valance of ion, F is Faraday constant, C_{out} is the concentration of ions outside of the membrane and C_{in} is the concentration of ions inside of the membrane (Table S4). Overall, their corresponding currents can be described as Eqs (13).

$$I_{K^+} = \overline{G_{K^+}} n^4 (V_m - E_{K^+})$$
$$I_{Na^+} = \overline{G_{Na^+}} m^3 h (V_m - E_{Na^+}) \quad (13)$$
$$I_{leak} = \overline{G_{Leak}} (V_m - E_{leak})$$

TABLE S2*. Variables used in the modified HH model (11, 13).*

Variable	Definition	Value	Units
$\boldsymbol{T}$	Temperature	variable (Initial temperature is 309.5 K)	[K]
$\boldsymbol{V_m}$	Membrane potential / potential difference between outer- and inner bulk medium	variable	[V]
$\boldsymbol{n, m, h}$	Open probability of potassium (n) and sodium (m, h) channels.	variable	-
$\boldsymbol{\alpha_{n/m/h}}$	Opening rate of specific gate	variable	[s^{-1}]
$\boldsymbol{\beta_{n/m/h}}$	Closing rate of specific gate	variable	[s^{-1}]
$\boldsymbol{\overline{G_{K^+}}}$	Maximum conductance of the potassium channel	360	[$S \cdot m^{-2}$]
$\boldsymbol{\overline{G_{Na^+}}}$	Maximum conductance of the sodium channel	1200	[$S \cdot m^{-2}$]
$\boldsymbol{\overline{G_{Leak}}}$	Maximum conductance of the leak current	3	[$S \cdot m^{-2}$]
$\boldsymbol{E_{K^+}}$	Reversal (or equilibrium) potential of the potassium channel	−0.0799	[V]

E_{Na^+}	Reversal (or equilibrium) potential of the sodium channel	0.0614	[V]
E_{Leak}	Reversal (or equilibrium) potential for the passive leakage	−0.0544	[V]

TABLE S3. Values used to calculate equilibrium potential and the capacitive current (14).

Ion	Intracellular concentration [M]	Extracellular concentration [M]	Radius of hydrated ion [m]
Na^+	1.5×10^{-2}	1.5×10^{-1}	4×10^{-10}
K^+	1.0×10^{-1}	5.0×10^{-3}	3×10^{-10}
Cl^-	1.3×10^{-2}	1.5×10^{-1}	3×10^{-10}
Ca^{2+}	2.0×10^{-7}	1.0×10^{-3}	6×10^{-10}

Effect of the wavelength of stimulation light

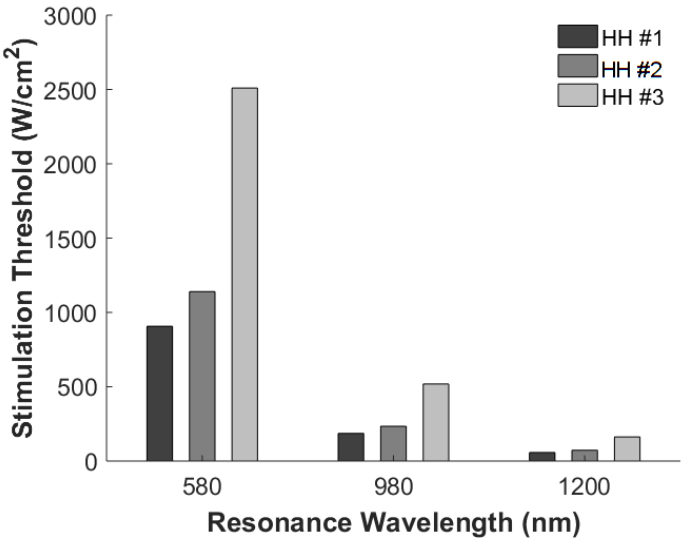

FIGURE S3. Stimulation thresholds in the models #1, #2, and #3 when different laser wavelengths are used. Stimulation duration, GNRs coverage, distance, and TRPV1 channel conductance are 0.5 ms, 0.031, 100 nm. and 2.1 $S \cdot m^{-2}$, respectively.

Supplementary References

1. Sassaroli, E., K.C. Li, and B.E. O'Neill. 2009. Numerical investigation of heating of a gold nanoparticle and the surrounding microenvironment by nanosecond laser pulses for nanomedicine applications. Phys Med Biol. 54: 5541–5560.

2. Papavassiliou, G.C. 1979. Optical Properties of Small Inorganic and Organic Metal Particles. Prog. Solid St. Chem. 12: 185–271.

3. Ni, W., X. Kou, Z. Yang, and J. Wang. 2008. Tailoring longitudinal surface plasmon wavelengths, scattering and absorption cross sections of gold nanorods. ACS Nano. 2: 677–686.

4. Eom, K., J. Kim, J.M. Choi, T. Kang, J.W. Chang, K.M. Byun, S.B. Jun, and S.J. Kim. 2014. Enhanced Infrared Neural Stimulation using Localized Surface Plasmon Resonance of Gold Nanorods. Small. 10: 3853–3857.

5. Carvalho-de-Souza, J.L., J.S. Treger, B. Dang, S.B.H. Kent, D.R. Pepperberg, and F. Bezanilla. 2015. Photosensitivity of neurons enabled by cell-targeted gold nanoparticles. Neuron. 86: 207–217.

6. Eom, K., C. Im, S. Hwang, S. Eom, T.-S. Kim, H.S. Jeong, K.H. Kim, K.M. Byun, S.B. Jun, and S.J. Kim. 2016. Synergistic combination of near-infrared irradiation and targeted gold nanoheaters for enhanced photothermal neural stimulation. Biomed. Opt. Express. 7: 1614–1625.

7. Voets, T., G. Droogmans, U. Wissenbach, A. Janssens, V. Flockerzi, and B. Nilius. 2004. The principle of temperature-dependent gating in cold- and heat-sensitive TRP channels. Nature. 430: 748–754.

8. Caterina, M.J., M.A. Schumacher, M. Tominaga, T.A. Rosen, J.D. Levine, and D. Julius. 1997. The capsaicin receptor: a heat-activated ion channel in the pain pathway. Nature. 389: 816–824.

9. Shapiro, M.G., K. Homma, S. Villarreal, C.-P. Richter, and F. Bezanilla. 2012. Infrared light excites cells by changing their electrical capacitance. Nat. Commun. 3: 736.

10. Malmberg, C.G., and A. a. Maryott. 1956. Dielectric constant of water from 0 to 100 C. J. Res. Natl. Bur. Stand. (1934). 56: 1.

11. Hodgkin, A.L., and A.F. Huxley. 1952. A quantitative description of membrane current and its application to conduction and excitation in nerve. J. Physiol. 117: 500–544.

12. Plaksin, M., E. Kimmel, and S. Shoham. 2017. Thermal transients excite neurons through universal intramembrane mechano-electrical effects. bioRxiv. .

13. Lee, J., D.A. Boas, and S.J. Kim. 2011. Multiphysics neuron model for cellular volume dynamics. IEEE Trans. Biomed. Eng. 58: 3000–3003.

14. Simons, T.J.B. 1988. Calcium and neuronal function. Neurosurg. Rev. 11: 119–129.